LA-UR-18-24332 (Accepted Manuscript)

Evolution of topological skyrmions across the spin reorientation transition in Pt/Co/Ta multilayers

He, Min; Li, Gang; Zhu, Zhaozhao; Zhang, Ying; Peng, Licong; Li, Rui; Li, Jianqi; Wei, Hongxiang; Zhao, Tongyun; Zhang, X.-G.; Wang, Shouguo; Lin, Shizeng; Gu, Lin; Yu, Guoqiang; Cai, Jianwang; Shen, Bao-gen

To be published in: Physical Review B

DOI to publisher's version: 10.1103/PhysRevB.97.174419

Permalink to record: http://permalink.lanl.gov/object/view?what=info:lanl-repo/lareport/LA-UR-18-24332

Tunable nontrival skyrmions in Pt/Co/Ta multilayers with magnetic anisotropy from exsy-axis to easy-plane

MinHe,[1,2] GangLi,[1,2] ZhaozhaoZhu,[1,2] YingZhang,[1,*] LicongPeng,[1,2] RuiLi,[1,2] JianqiLi,[1,2] HongxiangWei,[1] TongyunZhao,[1] X.-G Zhang.,[3] ShouguoWang,[4] Shi-Zeng Lin,[5] Lin Gu,[1,2] GuoqiangYu,[1] JianwangCai,[1,2,*] Bao-genShen[1]

[1] *Beijing National Laboratory for Condensed Matter Physics, Institute of Physics, Chinese Academy of Sciences, Beijing 100190, China*

[2]*School of Physical Sciences, University of Chinese Academy of Sciences, Beijing 100049, China*

[3]*Department of Physics and the Quantum Theory Project, University of Florida, Gainesville, FL 32611, United States*

[4]*Institute of Advanced Materials, Beijing Normal University, Beijing 100875, China*

[5]*Theoretical Division, Los Alamos National Laboratory, Los Alamos, New Mexico 87545, USA*

Magnetic skyrmions in multilayers are particularly appealing as next generation memory devices due to their topological compact size, the robustness against external perturbations, the capability of electrical driving and detection, and the compatibility with the existing spintronic technologies. To date, Néel-type skyrmions at room temperature (RT) have been studied mostly in multilayers with easy-axis magnetic anisotropy. Here, we systematically explore the evolution of magnetic skyrmions with sub-50 nm size in a series of Pt/Co/Ta multilayers where the magnetic anisotropy is tuned continuously from easy-axis to easy-plane by increasing the ferromagnetic Co layer thickness. The existence of nontrivial skyrmions are identified via the combination of in-situ Lorentz transmission electron microscopy (L-TEM) and Hall transport measurements. A high-density of magnetic skyrmions over a wide temperature range are observed in the multilayers with easy-plane anisotropy, which will stimulate further exploration for new materials and accelerate the development of skyrmion-based spintronic devices.

*zhangy@iphy.ac.cn; jwcai@aphy.iphy.ac.cn

I. INTRODUCTION

Magnetic skyrmions are swirling spin textures, which have attracted tremendous interests in the last decade, due to their nontrivial spin topology and novel physical properties that can be exploited for applications in spintronic devices [1]. These novel spin textures with integer topological number have been explored in various magnetic materials from bulk to thin films. The exchange interaction, the dipolar interaction, the Dzyaloshinskii-Moriya interaction (DMI) and the anisotropy compete with each other to stabilize nontrivial spin textures. For instance, interesting phenomena of magnetic domain formation have been previously revealed by tuning the interplay among magnetic interactions without considering the DMI [2,3]. The magnetic anisotropy has been shown to play an important role in determining the topological spin configuration. The magnetic domains like the traditional magnetic bubbles with narrow domain walls require a uniaxial anisotropy K_u to be greater than the shape anisotropy $K_d = 2\pi M_S^2$, i.e. the Q factor($Q = \frac{K_u}{K_d}$) should be larger than 1 [4]. For these films with Q>1, the domain morphology favors magnetization direction along the easy-axis, which is perpendicular to the thin film. The magnetization transition in the formation of magnetic stripe domain phase and magnetic bubbles has been studied at the spin reorientation transition (SRT) of the magnetic films with Q factor around 1 [3,4]. Recently, particle-like spin textures called magnetic skyrmions were firstly discovered in the magnetic materials without inversion center, where the skyrmions are stabilized by the competing DMI and ferromagnetic exchange interactions [5–7]. Because of their unique topology and weak pinning to the atomic crystal, skyrmions can be driven

efficiently by electric currents [8–10], resulting in low power dissipation compared to conventional domain wall.

Skyrmions have also been observed in thin films, where the mirror symmetry is explicitly broken. The skyrmions in thin films are particularly attractive because their spin-orbit coupling (SOC) and other magnetic interactions can be engineered conveniently via layer materials [11], layer thickness [12,13], and repetition numbers [14]. The enhanced SOC from heavy metals and the interfacial DMI from the symmetry-breaking structures can reduce the skyrmion sizes, stabilize skyrmions up to the room temperature and strengthen the interaction with flowing electrons [8,15–17]. Moreover, due to the compatibility with current spintronic fabrication techniques, room-temperature skyrmions in thin films can be readily integrated into the spintronic devices.

Previous works [8,9,11–14,18–21] including our recent work [22] focused on the scattered Néel-type skyrmions in the sandwiched magnetic multilayers with easy-axis anisotropy in the range of $Q > 1$, where the interfacial DMI stabilizes chiral magnetic domains. This is indeed in accordance with theoretical calculations, where an easy-axis anisotropy helps to stabilize skyrmions [23]. On the other hand, recent theoretical calculations and simulations have shown that the skyrmions in thin films survive even with an moderate easy-plane anisotropy and a new skyrmions square lattice might appear [24,25]. Skyrmion-like spin textures were observed in Fe/Gd films with easy-plane anisotropy, without knowing the detailed topology and the role of DMI [2]. To date, the skyrmions in the thin films with easy-plane anisotropy and interfacial DMI

has not been experimentally studied and the systematic correlation with typical Néel-type skyrmions is unknown.

Here, we extend our exploration to series of Pt/Co/Ta multilayers with interfacial DMI, where the smooth magnetic anisotropy transition from easy-axis to easy-plane occurs by increasing the Co layer thickness. The electrical transport measurements of the topological Hall effect (THE) together with the correponding magentic imaging via Lorentz transmission electron microscopy (L-TEM) unambiguously identify the nontrivial spin textures as magnetic skyrmions. The skyrmion density increases continuously with the Co layer thickness coinciding with the increase of easy-plane anisotropy to produce decreased domain wall width via Yafet's model [26]. The confirmation of nontrivial topological spin configuration in the films with broader range of anisotropy based on traditional magnetic structures and interfacial DMI could simplify and broaden the material choice for hosting skyrmions, and allow for optimizing the skyrmions properties for device applications.

II. EXPERIMENTS

The magnetic multilayers with core structure of Ta(4)/[Pt(3)/Co(t)/Ta(3)]$_6$ (where 6 denotes the layer repetition numbers, thickness in nm and Co-layer thickness t varying from 1.85 nm to 2.1 nm) were grown by magnetron sputtering on 10-nm-thick Si_3N_4 membrane windows for direct TEM observation and simultaneously on thermally oxidized Si wafers with standard Hall bar shape for transport property measurements. The structure is schematically shown in Fig. 1(a). The magnetic structures were observed by L-TEM (JEOL 2100F) with perpendicular magnetic fields applied by

gradually increasing the objective lens current. The magnetic hysteresis ($M-H$) loops of the Hall bars were measured using superconducting quantum interference device magnetometer (SQUID). Hall resistivity (ρ_{xy}) measurements were conducted in the same Hall bars with a small, non-perturbative constant current of 0.5 mA applied along the longitudinal direction (See Fig. S5 in supplementary material for the measurement and extraction details).

III. RESULTS

The magnetic anisotropy loops together with the corresponding magnetic domain morphology of the representative multilayers at room temperature are shown in Fig. 1 (See Fig. S1 for more multilayers in supplementary material). For multilayers with thinner Co layer thickness $t_{Co} = 1.85\ \text{nm}$ shown in Fig. 1(b), significant easy-axis anisotropy is observed from the magnetic hysteresis loops. With increasing Co layer thickness, easy-axis anisotropy becomes comparable to easy-plane anisotropy and nearly equal saturate fields along both the perpendicular and in-plane directions are measured in the multilayer with $t_{Co} = 1.95\ \text{nm}$ as shown in Fig. 1(c). With further increasing Co layer thickness, the typical easy-plane anisotropy is dominated based on the magnetic hysteresis loop of $t_{Co} = 2.1\ \text{nm}$ multilayer as shown in Fig. 1(d). The smooth crossover from easy-axis to easy-plane while increasing Co layer thickness indicates that the perpendicular magnetization originates from the interfacial effect [4,27,28]. More interestingly, the multilayers with easy-plane anisotropy exhibit denser magnetic stripe domains (See Fig. S2 of supplementary material), which evolve into high-density skyrmion-like magnetic domains under perpendicular magnetic fields.

The magnetic domain evolution under magnetic fields (See Fig. S3 in supplementary material) is similar to the previous reports about the magnetic skyrmions and bubbles [14,29]. The magnetic stripes completely transform into skyrmion-like domains (~50 nm) at an optimized magnetic field of 680, 930, and 1040 Oe, as shown in Figs. 1(e)–1(g). Further increasing the magnetic field above the critical value of about 890, 1190 and 1600 Oe, the ferromagnetic phase is obtained, corresponding to the saturation fields along the perpendicular direction. The required magnetic field to generate and annihilate the skyrmion-like domains is significantly enhanced in the multilayers with easy-plane anisotropy. Remarkably, the high-density stripes and skyrmion-like domains are beyond the expectation of large magnetic domains for common easy-plane material (See the large magnetic domains in Fig. S4 of supplementary material).

To determine the topology of the observed spin texture, we further performed the magneto-transport measurements. An emergent magnetic field is produced when the conduction electrons interact with the skyrmions, which yields the topological Hall effect [30–32]. The emergent magnetic field is proportional to the skyrmion topological charge density. The measured Hall resistivity can be attributed to the ordinary Hall effect (OHE), anomalous Hall effect (AHE), and THE [30–32], i.e., $\rho_{xy} = R_0 H + R_S M + \rho_{TH}$, where R_0 is the ordinary Hall coefficient, R_S is the anomalous Hall coefficient that is approximately in dependent on the magnetic fields. M is the out-of-plane magnetization, and ρ_{TH} is the topological Hall resistivity (THR). The out-of-plane magnetic hysteresis loop and the total Hall resistivity for the Hall bar-

shape multilayers with $t_{Co} = 1.95$ nm are shown in Figs. 2(a)-2(b). The individual resistivity contribution from OHE, AHE and THE components is separately derived from the total Hall resistivity as in Fig. 2(c) (See details in Fig. S5 of supplementary material). The dependence of ρ_{TH} on Co-layer thickness is summarized in Fig. 2(d) with the opposite sign across zero field [33] and the significant THE is identified by the striking hump-like peaks at a certain magnetic field. The ρ_{TH} peak shifts toward higher magnetic fields for the multilayers with thicker Co layer, in good agreement with the increased magnetic fields via L-TEM observation (Fig. 1). Thus from the topological Hall signal, the observed spin textures are determined as nontrivial skyrmions. The broader ρ_{TH} peak consists with the broader range of magnetic field for the existence of skyrmions in the multilayers with thicker Co layer. The maximum THR value is extracted and summarized for different Co layer thickness in Fig. 2(e). Interestingly, the maximum THR value of~ 170 nΩ·cm in the multilayers ($t_{Co} = 1.85$ nm) with easy-axis anisotropy is slightly larger than those in chiral FeGe epitaxial films (~160 nΩ·cm) and Mn_5Si_3 films (~50 nΩ·cm) [31,34], despite the fact that Néel-type skyrmions in multilayers with easy-axis anisotropy have significantly lower density than the Bloch-type skyrmion lattice in chiral bulk magnets. The spin configuration may influence the THR value besides the dominant skyrmion density, which is further confirmed by the slightly decreased THR maximum value for higher-density skyrmions in the multilayers while the magnetic anisotropy transforming to easy-plane.

Next, the spin configuration evolution with Co layer thickness are analyzed at RT

by tilting the specimen based on the magnetic field-induced beam deflection and the contrast mechanism of L-TEM [35]. Néel-type skyrmions have been theoretically and experimentally distinguished by this method [36], which can be summarized as the disappearance of contrast at a position and reversal of contrast at relatively opposite angles. The tilting procedure is schematically illustrated in Fig. 3(a). The enlarged images of a selected single skyrmion are shown in insets, where the reversed bright and dark magnetic contrasts at relatively opposite tilting angle of 18° (Figs. 3(b)-3(d)) are clearly observed with no contrast at zero tilting angle (Fig. 3(c)) for the multilayer with $t_{\mathrm{Co}} = 1.85$ nm. These contrast features correspond well to the typical Néel-type skyrmions in multilayers with an easy-axis anisotropy [36]. Therefore, Néel-type magnetic skyrmions are successfully identified in the above Pt/Co/Ta multilayers based on the topological Hall resistivity and their response to a tilted angle. By increasing Co layer thickness to 1.95 nm, only a few Néel-type skyrmions can be identified as marked by yellow arrows in Figs. 3(e)-3(g) using the same tilting procedure. The consistent contrast regardless of any tilting angle indicates non-ideal Néel-type skyrmions (probably in the transition to Bloch-type). These non-ideal Néel-type skyrmions become dominant in the easy-plane multilayer ($t_{\mathrm{Co}} = 2.1$ nm) as shown in Figs. 3(h)-3(j).

Furthermore, the correlation between THR asymmetry and microscopic skyrmion evolution is investigated with increasing/decreasing magnetic fields in Pt/Co(2.0)/Ta multilayers with an easy-plane anisotropy. The results are shown in Fig. 4. The THR peak shows a slight shift to lower magnetic fields and the resistivity magnitude is

lowered while decreasing the magnetic fields from saturation (Fig. 4(a)). Correspondingly, less skyrmions are observed at an optimized magnetic field of 920 Oe while decreasing the magnetic fields in comparison to that at an optimized 950 Oe when increasing the fields as shown in Figs. 4(d)-4(f), respectively. The gradual appearance of skyrmions in a field range (from 990 to 570 Oe) is observed (Figs. 4(e)-4(g) when decreasing the magnetic fields, which is slightly narrower than the THR peak.

The thermal stability of high-density skyrmions in the multilayers with easy-plane anisotropy ($t_{\mathrm{Co}} = 2.1$ nm) is investigated via in-situ cooling L-TEM. Robust skyrmions are observed over a wide temperature range (12–300 K) as shown in Fig. 5, (the approachable temperature range for our LTEM). The skyrmion number density in the $H - T$ plane is displayed in in Fig. 5(d). The magnetic fields required to create and annihilate skyrmions are approximately constant during the whole temperature range investigated here. Based on the above results, the high-density skyrmions in the multilayers with easy-plane anisotropy are stable over a wide temperature range including room temperature, which is advantageous for applications.

IV. DISCUSSION

The stripe domain evolution during the smooth crossover from easy-axis to easy-plane anisotropy by increasing Co layer thickness in series of Pt/Co/Ta multilayers is similar to traditional spin reorientation transition in an ultrathin magnetic film [4,37]. By considering the magnetic exchange interaction, magnetic anisotropy, dipolar interaction, and the Zeeman energy, Yafet's model can be used to calculate the stripe width and domain wall width [26,37]. The stripe domain width decreases with

decreasing perpendicular magnetic anisotropy, which explains the denser magnetic stripes and skyrmions in easy-plane multilayers of $t_{\mathrm{Co}} = 2.1$ nm (See Fig. S2 and Fig. S3 of supplementary material). Different from the irregular micro-size magnetic bubbles evolved from stripes at SRT of traditional Fe/Ni/Cu film, the magnetic domains in these series of Pt/Co/Ta multilayers are homogeneous and small (~50 nm) under certain magnetic fields. The different interfacial Co/Pt and Co/Ta structures introduces net DMI and the chiral Néel-type skyrmions has been confirmed in the Pt/Co/Ta mulitlayers with easy-axis anisotropy [9,11,38]. The increased Co layer thickness diminishes the interfacial DMI but still contributes to the nontrivial chirality in the multilayer with easy-plane anisotropy, which is verified by the prominent THR peaks and LTEM identification. Moreover, no expanding or shrinking features of the S=0 magnetic bubbles [8] are observed under the electric current stimulation. The competition between the decreased DMI and increased dipolar interaction can stabilize skyrmions with intermediate helicity, other than the Néel (helicity=0 or pi) or Bloch skyrmions (helicity=+-pi/2). This is because the dipolar interaction favors Bloch-type skyrmions while the interfacial DMI favors Néel-type skyrmions [9]. The evolution of spin textures with Co thickness is similar to the theoretically-predicted Néel-to-Bloch spin configuration transition caused by the magnetization switch from perpendicular direction to in-plane [9]. However, it is very difficult to identify the detailed spin configuration of those non-ideal Néel skyrmions due to the complicated spin transformation [36] and the limitation of L-TEM technique, which is capable of showing only the in-plane magnetization. The compromise between perpendicular field

and easy-plane anisotropy [24] together with DMI favors the spin arrangements of skyrmions, which are further confirmed by the topological Hall resistivity measurement and the increased skyrmion density. In addition to the contribution from skyrmion density, the sign and strength of THR can also be determined by electronic structures [39,40] and other spin configurations. The microscopic correlation between the observed skyrmion evolution and the topological properties is revealed via in-situ LTEM in the multilayers $t_{\mathrm{Co}} = 2.1\ \mathrm{nm}$ with an easy-plane anisotropy, indicating the hysteresis effects based on the slightly lowered magnetic field required for the complete skyrmion state. The significant hysteresis and narrow THR peak range in the multilayers $t_{\mathrm{Co}} = 1.85\ \mathrm{nm}$ with easy-axis make it difficult to observe the intermediate skyrmion phase by sweeping the magnetic fields (See Figs. S6-S7 in the supplementary material). Therefore, the above experimental THR results call for further theoretical study on the origin of the topological Hall effect in the multilayers. The robustness of skyrmions against thermal disruption has been demonstrated in the broad temperature range of 12K-300K. The slightly lower skyrmion density at lower temperature is probably due to the magnetic anisotropy increase or lower thermal activation rate for skyrmions [41]. In contrast, skyrmions only exist within narrow temperature range near Curie temperature (T_{C}) in B20 alloys [5,6] and the density decreases significantly while the temperature drops away from T_{C} in the dipolar-determined bulk MnNiGa sample [41].

In conclusion, nontrivial skyrmions with sub-50 nm size and continuously tunable density have been observed and studied systematically via the combination of the in-

situ Lorentz transmission electron microscopy (L-TEM) and magnetic transport measurements in series of Pt/Co/Ta multilayers. The topological nontrivial high-density skyrmions in multilayers with an easy-plane anisotropy are robust in the temperature range of 12-300 K. The direct microscopic relationship between the topological Hall resistivity and the evolution of magnetic field-induced skyrmions is established. The discovery of skyrmions by combining the interfacial DMI with traditional magnetic structures could simplify and broaden the material choice for hosting skyrmions and allow for optimizing the skyrmions properties for device applications.

ACKNOWLEDGMENTS

We thank Dr. Liqian Ke from Ames Lab for his helpful discussion. This work was supported by the National Key Research and Development Program of China (No. 2016YFA0300804), the National Natural Science Foundation of China (Grant Nos. 51590880, 51431009, 11674373 and 51625101), and the Youth Innovation Promotion Association of CAS (No. 2015004).

ADDITIONAL INFORMATION

See Supplemental Material at [URL will be inserted by publisher].

References

[1] N. Nagaosa and Y. Tokura, Nat. Nanotech. **8**, 899 (2013).

[2] S. A. Montoya, S. Couture, J. J. Chess, J. C. T. Lee, N. Kent, D. Henze, S. K. Sinha, M. Y. Im, S. D. Kevan, P. Fischer, B. J. McMorran, V. Lomakin, S. Roy, and E. E. Fullerton, Phys. Rev. B **95**, 024415 (2017).

[3] J. Choi, J. Wu, C. Won, Y. Z. Wu, A. Scholl, A. Doran, T. Owens, and Z. Q. Qiu, Phys. Rev. Lett. **98**, 207205 (2007).

[4] M. Kisielewski, A. Maziewski, T. Polyakova, and V. Zablotskii, Phys. Rev. B **69**, 184419 (2004).

[5] S. Mühlbauer, B. Binz, F. Jonietz, C. Pfleiderer, A. Rosch, A. Neubauer, R. Georgii, and P. Böni, Science **323**, 915 (2009).

[6] W. Münzer, A. Neubauer, T. Adams, S. Mühlbauer, C. Franz, F. Jonietz, R. Georgii, P. Böni, B. Pedersen, M. Schmidt, A. Rosch, and C. Pfleiderer, Phys. Rev. B **81**, 41203 (2010).

[7] X. Z. Yu, N. Kanazawa, Y. Onose, K. Kimoto, W. Z. Zhang, S. Ishiwata, Y. Matsui, and Y. Tokura, Nat. Mater. **10**, 106 (2011).

[8] W. J. Jiang, P. Upadhyaya, W. Zhang, G. Q. Yu, M. B. Jungfleisch, F. Y. Fradin, J. E. Pearson, Y. Tserkovnyak, K. L. Wang, and O. Heinonen, Science **349**, 283 (2015).

[9] S. Woo, K. Litzius, B. Kruger, M. Y. Im, L. Caretta, K. Richter, M. Mann, A. Krone, R. M. Reeve, M. Weigand, P. Agrawal, I. Lemesh, M. A. Mawass, P. Fischer, M. Klaui, and G. S. Beach, Nat. Mater. **15**, 501 (2016).

[10] G. Q. Yu, P. Upadhyaya, X. Li, W. Li, S. K. Kim, Y. Fan, K. L. Wong, Y. Tserkovnyak, P. K. Amiri, and K. L. Wang, Nano. Lett. **16**, 1981 (2016).

[11] A. Soumyanarayanan, M. Raju, A. L. G. Oyarce, A. K. C. Tan, M.-Y. Im, A. P. Petrovic, P. Ho, K. H. Khoo, M. Tran, C. K. Gan, F. Ernult, and C. Panagopoulos, Nat. Mater. **16**, 898 (2017).

[12] G. Q. Yu, P. Upadhyaya, X. Li, W. Li, S. K. Kim, Y. Fan, K. L. Wong, Y. Tserkovnyak, P. K. Amiri, and K. L. Wang, Nano. Lett. **16**, 1981 (2016).

[13] G. Chen, A. Mascaraque, A. T. N'Diaye, and A. K. Schmid, Appl. Phys. Lett. **106**, 242404 (2015).

[14] C. Moreau-Luchaire, S. C. Mouta, N. Reyren, J. Sampaio, C. A. Vaz, N. V Horne, K. Bouzehouane, K. Garcia, C. Deranlot, P. Warnicke, P. Wohlhuter, J. M. George, M. Weigand, J. Raabe, V. Cros, and A. Fert, Nat. Nanotech. **11**, 444 (2016).

[15] A. Fert and P. M. Levy, Phys. Rev. Lett. **44**, 1538 (1980).

[16] A. Crepieux and C. Lacroix, J. Magn. Magn. Mater. **182**, 341 (1998).

[17] A. Fert, Mater. Sci. Forum **59-60**, 439 (1990).

[18] O. Boulle, J. Vogel, H. Yang, S. Pizzini, D. de S. Chaves, A. Locatelli, T. O. Mentes, A. Sala, L. D. Buda-Prejbeanu, O. Klein, M. Belmeguenai, Y. Roussigne, A. Stashkevich, S. M. Cherif, L. Aballe, M. Foerster, M. Chshiev, S. Auffret, I. M. Miron, and G. Gaudin, Nat. Nanotech. **11**, 449 (2016).

[19] L. Sun, R. X. Cao, B. F. Miao, Z. Feng, B. You, D. Wu, W. Zhang, A. Hu, and H. F. Ding, Phys. Rev. Lett. **110**, 167201 (2013).

[20] W. J. Jiang, X. C. Zhang, G. Q. Yu, W. Zhang, X. Wang, M. B. Jungfleisch, J. E. Pearson, X. M. Cheng, O. Heinonen, K. L. Wang, Y. Zhou, A. Hoffmann, and S. G. E. te Velthuis, Nat. Phys. **13**, 162 (2016).

[21] G. Q. Yu, P. Upadhyaya, Q. Shao, H. Wu, G. Yin, X. Li, C. He, W. Jiang, X. Han, P. K. Amiri, and K. L. Wang, Nano. Lett. **17**, 261 (2017).

[22] M. He, L. Peng, Z. Zhu, G. Li, J. Cai, J. Li, H. Wei, L. Gu, S. Wang, T. Zhao, B. Shen, and Y. Zhang, Appl. Phys. Lett. **111**, 202403 (2017).

[23] A. B. Butenko, A. A. Leonov, U. K. Rößler, and A. N. Bogdanov, Phys. Rev. B **82**, 052403 (2010).

[24] S. Banerjee, J. Rowland, O. Erten, and M. Randeria, Phys. Rev. X **4**, 031045 (2014).

[25] S. Z. Lin, A. Saxena, and C. D. Batista, Phys. Rev. B **91**, 224407 (2015).

[26] Y. Yafet and E. M. Gyorgy, Phys. Rev. B **38**, 9145 (1988).

[27] M. Kisielewski, A. Maziewski, M. Tekielak, A. Wawro, and L. T. Baczewski, Phys. Rev. Lett. **89**, 87203 (2002).

[28] M. J. Johnson, P. J. H. Bloemen, F. J. A. den Broeder, and J. J. de Vries, Rep. Prog. Phys. **59**, 1409 (1996).

[29] N. Romming, C. Hanneken, M. Menzel, J. E. Bickel, B. Wolter, K. von Bergmann, A. Kubetzka, and R.Wiesendanger, Science **341**, 636 (2013)

[30] N. Kanazawa, Y. Onose, T. Arima, D. Okuyama, K. Ohoyama, S. Wakimoto, K. Kakurai, S. Ishiwata, and Y. Tokura, Phys. Rev. Lett. **106**, 156603 (2011).

[31] S. X. Huang and C. L. Chien, Phys. Rev. Lett. **108**, 267201 (2012).

[32] N. A. Porter, J. C. Gartside, and C. H. Marrows, Phys. Rev. B **90**, 24403

(2014).

[33] J. C. Gallagher, K. Y. Meng, J. T. Brangham, H. L. Wang, B. D. Esser, D. W. McComb, and F. Y. Yang, Phys. Rev. Lett. **118**, 27201 (2017).

[34] C. Sürgers, G. Fischer, P. Winkel, and H. v. Löhneysen, Nat. Commun. **5**, 6 (2014).

[35] M. J. Benitez, A. Hrabec, A. P. Mihai, T. A. Moore, G. Burnell, D. McGrouther, C. H. Marrows, and S. McVitie, Nat. Commun. **6**, 8957 (2015).

[36] S. D. Pollard, J. A. Garlow, J. Yu, Z. Wang, Y. Zhu, and H. Yang, Nat. Commun. **8**, 14761 (2017).

[37] Y. Z. Wu, C. Won, A. Scholl, A. Doran, H. W. Zhao, X. F. Jin, and Z. Q. Qiu, Phys. Rev. Lett. **93**, 117205 (2004).

[38] A. Fert, N. Reyren, and V. Cros, Nat. Rev. Mater. **2**, 17031 (2017).

[39] A. Neubauer, C. Pfleiderer, B. Binz, A. Rosch, R. Ritz, P. G. Niklowitz, and P. Boni, Phys. Rev. Lett. **102**, 186602 (2009).

[40] P. Bruno, V. K. Dugaev, and M. Taillefumier, Phys. Rev. Lett. **93**, 96806 (2004).

[41] L. Peng, Y. Zhang, W. Wang, M. He, L. Li, B. Ding, J. Li, Y. Sun, X. G. Zhang, J. Cai, S. Wang, G. Wu, and B. Shen, Nano Lett. **17**, 7075 (2017)

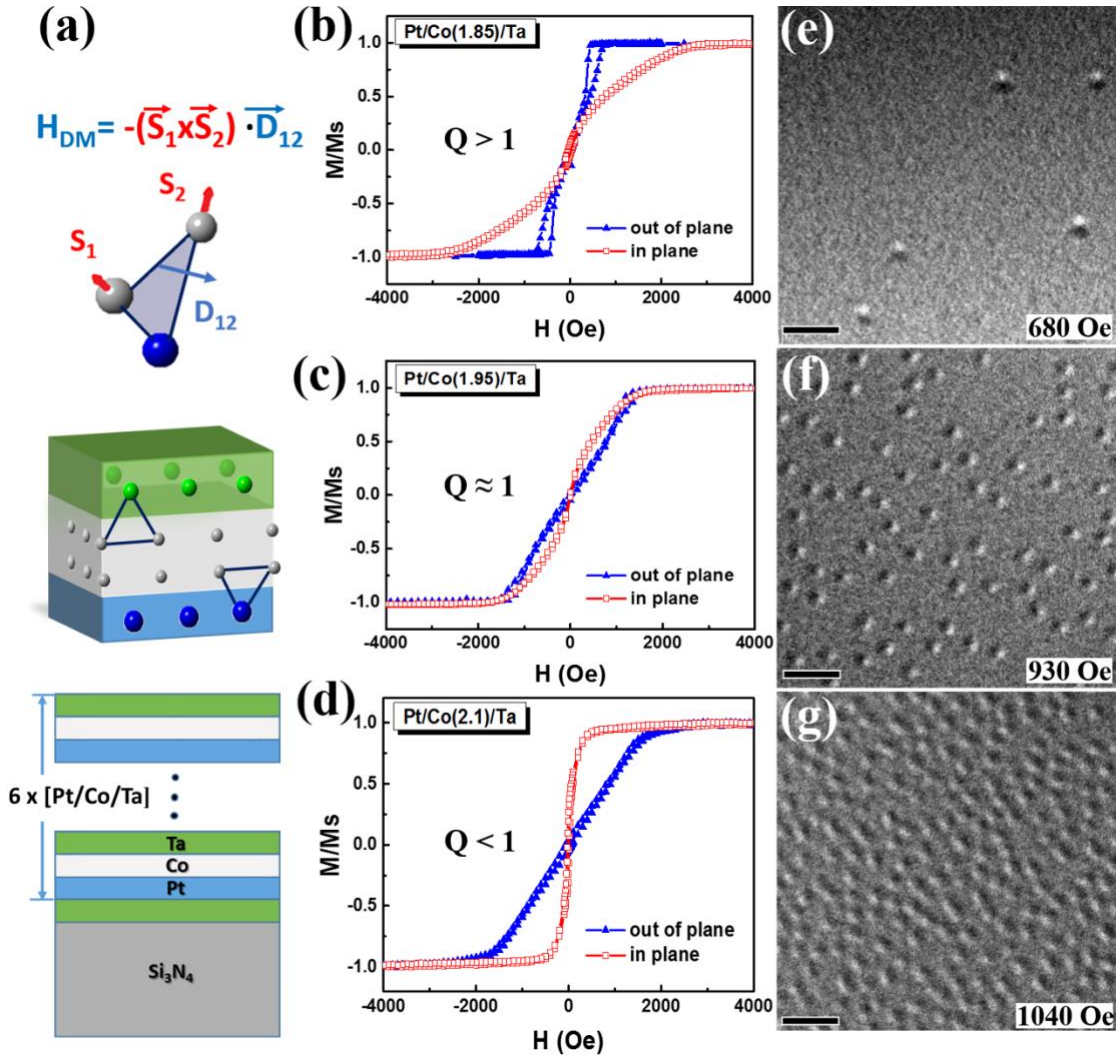

FIG. 1. The magnetic anisotropy together with the corresponding skyrmion distribution in Pt/Co/Ta multilayers. (a) Top: The DMI for two magnetic atoms (grey spheres) close to an atom (blue sphere) with a large spin–orbit coupling. Bottom: schematic multilayers made of six repetitions of the Pt/Co/Ta trilayer. (b)-(d) Room-temperature magnetic hysteresis loops measured along the in-plane and out-of-plane directions respectively. Each loop is normalized to saturate magnetization. (e)-(g) Magnetic skyrmion distribution while completely evolved from stripe domain at the magnetic fields of 680, 930 and 1040 Oe, respectively. The skyrmion density gets higher with thicker Co layer. The scale bar in (e)-(g) is 200 nm.

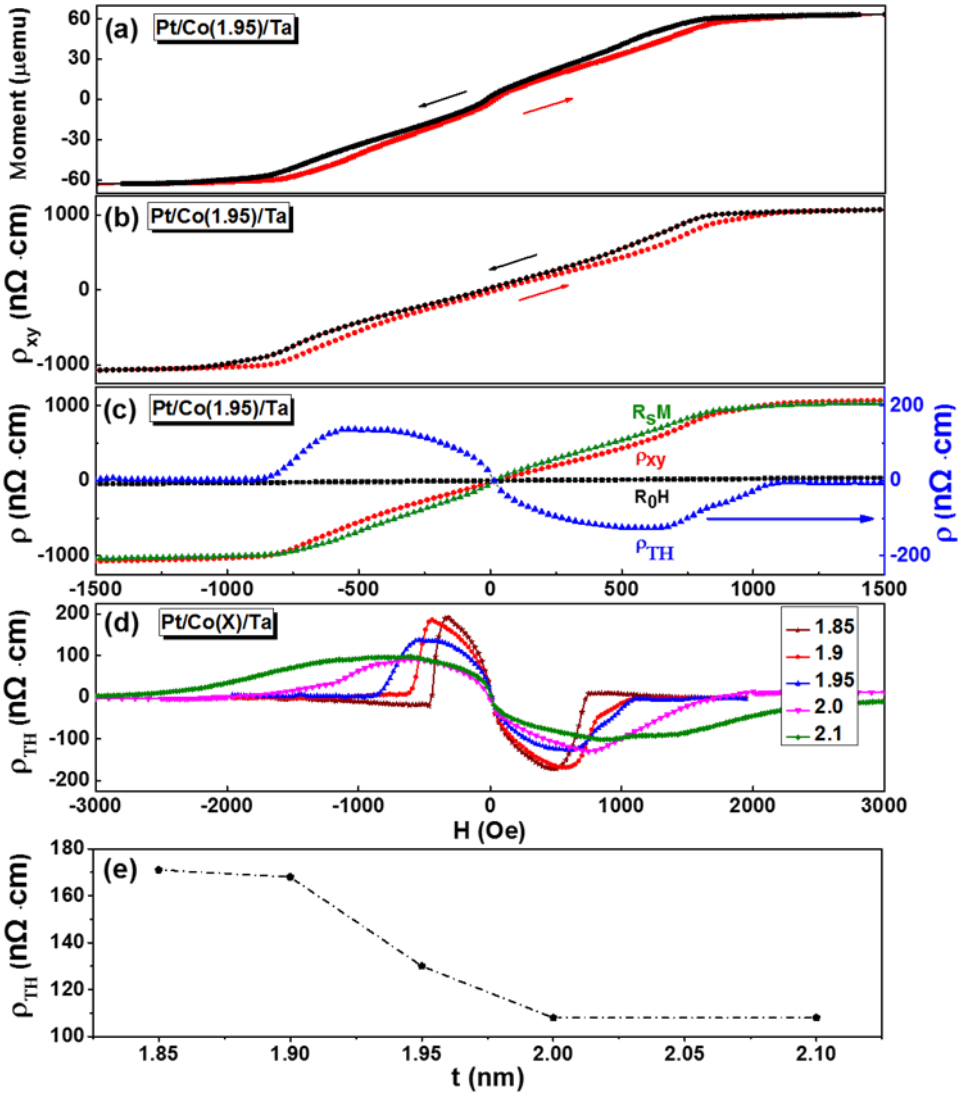

FIG. 2. The analysis of topological Hall resistivity (THR). (a) Out-of-plane magnetic hysteresis loop, (b) Total Hall resistivity (ρ_{xy}), and (c) THR (ρ_{TH}) extracted by subtracting ordinary resistivity (R_0H) and anomalous Hall resistivity (R_SM) from the experimental $\rho_{xy} - H$ curve in the representative Pt/Co(1.95)/Ta multilayers. (d) The summarized THR for the multilayers with various Co-layer thicknesses. (e) The maximum THR value dependent on the Co layer thickness.

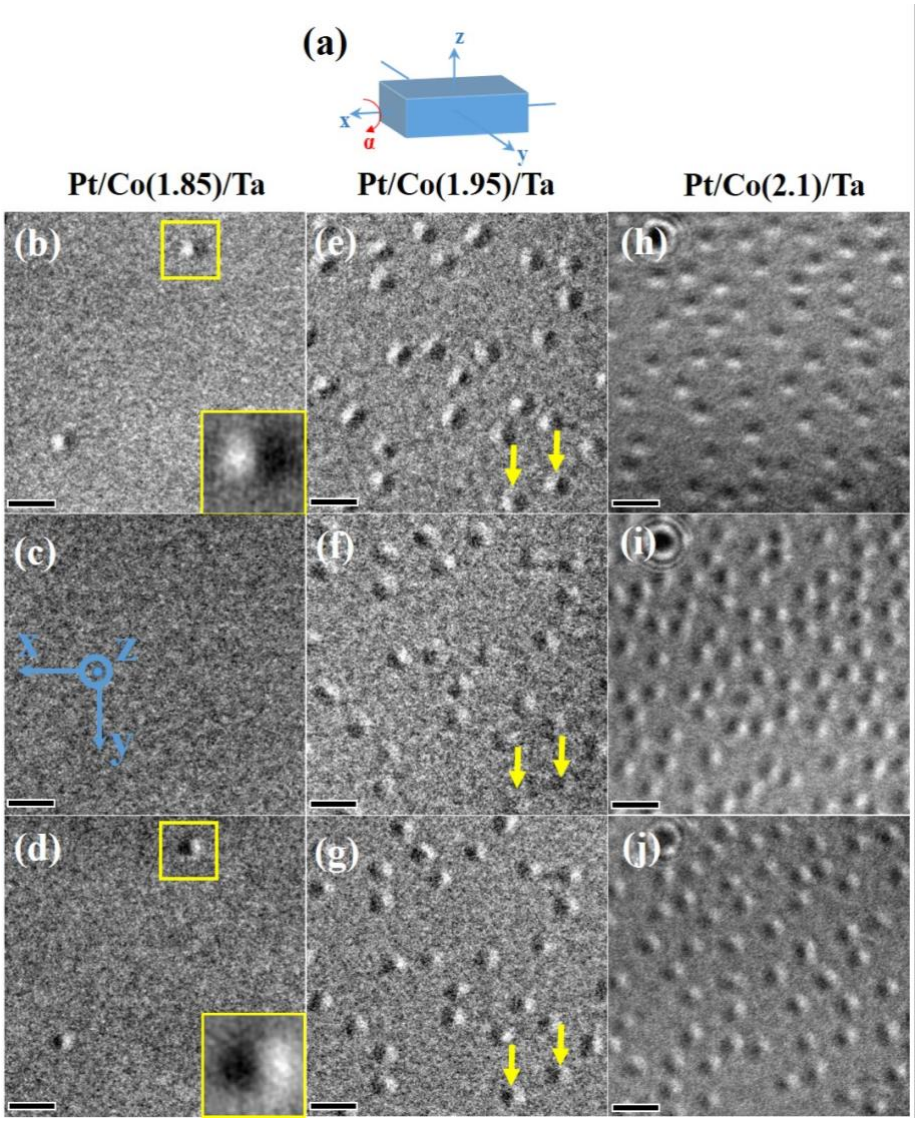

Fig. 3. Identification of skyrmion spin configuration by tilting samples in real-space L-TEM at RT. (a) Schematic diagram of titling process, α is the tilt angle around X-axis. The angle α for Pt/Co(1.85)/Ta is (b) -18°, (c) 0° and (d) 18°, respectively. The enlarged views of a single skyrmion in the insets (b) and (d) with bright and dark reversed magnetic contrast for the opposite tilting angle, identified as Néel-type skyrmion. The tilting angle α are (e) -18°, (f) 0° and (g) 18° for Pt/Co(1.95)/Ta, respectively. The tilting angle α are (h) -20°, (i) 0°and (j) 20° for Pt/Co(2.1)/Ta, respectively. Scale bars in (b)-(j) correspond to 50 nm.

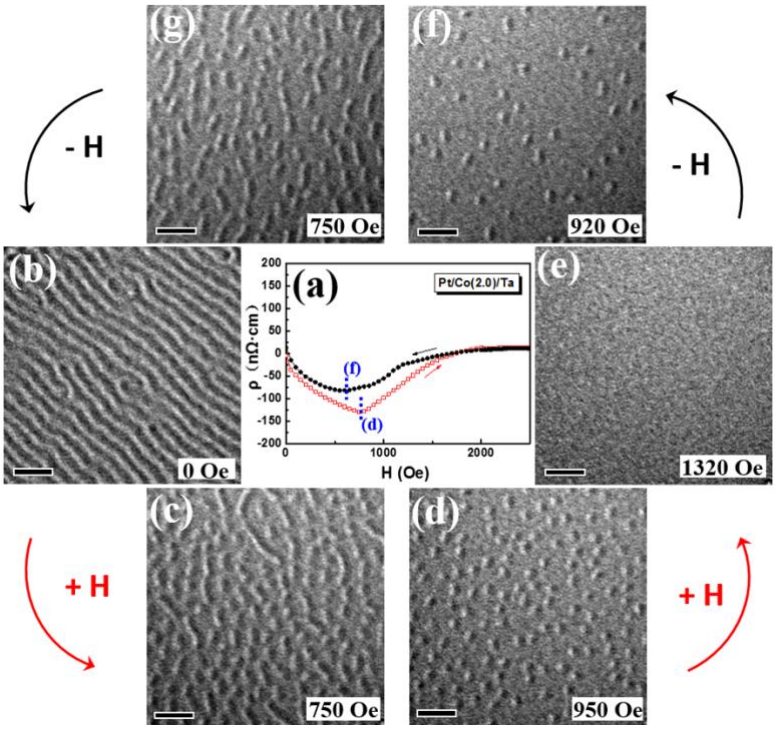

FIG. 4. The correlation between THR asymmetry and microscopic skyrmion evolution during increasing/decreasing magnetic fields in a representative Pt/Co(2.0)/Ta multilayers with IPA. (a) THR hysteresis loop. L-TEM images for the corresponding skyrmion evolution at different magnetic fields (b) 0 Oe, (c) 750 Oe, (d) 950 Oe, (e) 1320 Oe while increasing the magnetic field to saturation state, and (f) 920 Oe, (g) 750 Oe while decreasing the magnetic field. The scale bar in (b)-(g) is 200 nm.

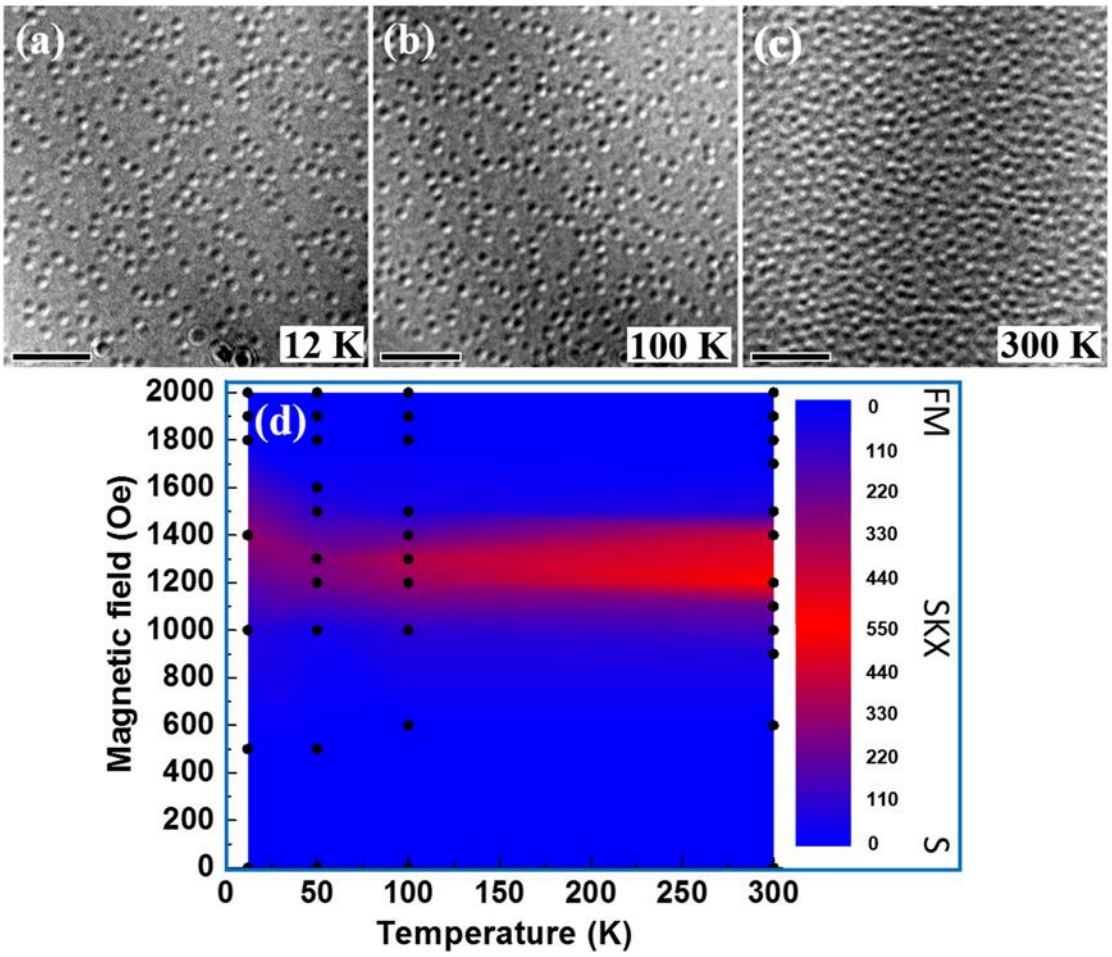

FIG. 5. Thermal stability of high-density skyrmions in Pt/Co(2.1)/Ta multilayers with IPA. L-TEM Fresnel images of magnetic skyrmions at different temperatures (a) 12 K, (b) 100 K and (c) 300 K. (d) The contour mapping of skyrmion density as a function of applied magnetic fields (H) and the temperature (T). The black dots show the experimental points, from which the skyrmion density map are extrapolated. The color scale indicates the skyrmion numbers per square micrometer. S for the stripe, SKX for skyrmions and FM for ferromagnetic state. The scale bar in (a)-(c) is 200 nm.